

University of Groningen

Novel phases in ferroelectric BaTiO₃ thin films

Everhardt, Arnoud

IMPORTANT NOTE: You are advised to consult the publisher's version (publisher's PDF) if you wish to cite from it. Please check the document version below.

Document Version

Publisher's PDF, also known as Version of record

Publication date:

2017

[Link to publication in University of Groningen/UMCG research database](#)

Citation for published version (APA):

Everhardt, A. (2017). *Novel phases in ferroelectric BaTiO₃ thin films: Enhanced piezoelectricity and low hysteresis*. Rijksuniversiteit Groningen.

Copyright

Other than for strictly personal use, it is not permitted to download or to forward/distribute the text or part of it without the consent of the author(s) and/or copyright holder(s), unless the work is under an open content license (like Creative Commons).

The publication may also be distributed here under the terms of Article 25fa of the Dutch Copyright Act, indicated by the "Taverne" license. More information can be found on the University of Groningen website: <https://www.rug.nl/library/open-access/self-archiving-pure/taverne-amendment>.

Take-down policy

If you believe that this document breaches copyright please contact us providing details, and we will remove access to the work immediately and investigate your claim.

Downloaded from the University of Groningen/UMCG research database (Pure): <http://www.rug.nl/research/portal>. For technical reasons the number of authors shown on this cover page is limited to 10 maximum.

Chapter 6:

Intrinsic hysteresis-free ferroelectric switching

Chapter to be submitted as peer- review article by A.S. Everhardt¹, T. Denneulin², A. Grünebohm³, Y.-T. Tsun⁴, S. Matzen⁵, N. Domingo⁶, S.-L. Zhou¹, E. Snoeck², M. Hÿtch², J.-M. Zuo⁴, Catalan^{6,7} and B. Noheda¹

¹ Zernike Institute for Advanced Materials, University of Groningen, The Netherlands

² CEMES-CNRS, F-31055 Toulouse Cedex 4, France

³ Faculty of Physics and CENIDE, University of Duisburg-Essen, 47048 Duisburg, Germany

⁴ Department of Materials Science and Engineering, University of Illinois, Urbana, Illinois, USA

⁵ Center for Nanoscience and Nanotechnology, Université Paris-Sud, CNRS, Université Paris-Saclay, Orsay, France

⁶ Catalan Institute of Nanoscience and Nanotechnology (ICN2), CSIC, Barcelona Institute of Science and Technology Campus, Universitat Autònoma de Barcelona, Bellaterra, 08193 Barcelona, Spain

⁷ ICREA, 08193 Barcelona, Spain

Abstract

Phase transitions are among the most interesting and ubiquitous phenomena in nature. In material science, they are responsible for the technological impact of ferromagnets, ferroelectrics, shape-memory alloys or memristors. Phase transitions are associated to desirably large, nonlinear changes in the order parameters (polarization, magnetization, resistance, etc) and susceptibilities, but at the same time they are often coupled to the presence of hysteresis, which is related to energy losses. In this chapter a route to intrinsic, hysteresis-free ferroelectric polarization switching is reported in these BaTiO₃ thin films without the need for chemical doping which is a requirement for all other low-hysteresis materials in literature. The 'slim', essentially temperature-independent ferroelectric hysteresis loop and large dielectric constant (~4000) give rise to fully reversible out-of-plane polarization switching with gradual rotation of the polarization, in contrast to large, anisotropic hysteresis in-plane switching with a divergent dielectric constant (maximum 40,000). The in-plane transition temperature can be brought down from 130 °C to 50 °C by changing the measurement direction, corresponding to the disappearance of b-polarization. Stabilization of an intermediate in-plane polarized stage for the out-of-plane direction also reveals a route towards an almost perfect realization of a strain diode with a five-fold increase of the piezoresponse, which reaches 100 pm/V.

6.1 Introduction

The change of external stimuli (temperature, electric or magnetic field, stress, etc.) in the proximity of a phase transition induces a change in basically all the relevant physical properties of a particular system, such as the order parameters (density, magnetization, polarization, strain, etc.) and susceptibilities. Some phase transitions display a continuous change of the order parameter (second order), but most often the phase change is discontinuous (first order). First order phase transitions take place by nucleation and growth of one phase into the other and this generation of nuclei is responsible for latent heat and the presence of metastable states in which the system gets trapped, giving rise to the phenomenon of hysteresis. Hysteresis is the difference in the magnitude of a property of the system between increasing and decreasing the external stimulus. A defining characteristic of many materials of interest in electronics and spintronics, such as in ferromagnets, ferroelectrics^[1] or memristors, is the resulting hysteresis loop under electric or magnetic fields^[2]. In particular, hysteresis is the key feature behind current information storage media as it provides the possibility for switching between two stable ground states.^[3] However, in many other applications, the desired feature of such electronic systems is the large, and often non-linear, response that comes together with the induced phase transition. In fact, hysteresis can be detrimental as it is associated to losses, for example in electro^[4] and magneto-caloric cooling^[5] where hysteresis loss lowers the efficiency; in high energy density capacitors where larger hysteresis reduces the stored energy for the same amount of work^[6], and piezoelectric sensors and actuators where hysteresis prevents stable and predictable operation^[7].

Electronic materials displaying low hysteresis are wanted for the design of many energy efficient applications, and the control of hysteresis in simple ferromagnetic systems has already reached a mature state.^[8] However, there are only limited tools to obtain hysteresis-free materials in complex first-order structural-magnetic phase transitions^[9] and ferroelectrics. Ferroelectric switching is dictated by nucleation and growth of one polar orientation into another one under the application of an electric field, where the hysteresis is dictated by the electric field required to overcome the energy barrier between the two orientations, the coercive field (**Figure 6.1**). Switching ferroelectric polarization is done either by directly nucleating domains with opposite, 180 ° difference, polarization, by two successive steps of 90 ° switching^[10–16], or by switching between different crystal phases^[17]. Hysteresis-free switching is so far only possible by being close to a phase transition. One approach is by going to the transition temperature^[6,18–24] which however limits the temperature stability and range. The second approach is by using chemical doping to get relaxor behavior or to get a Morphotropic Phase Boundary (MPB), which introduces extrinsic effects and additional disorder and, thus, limits their control and the understanding of the mechanisms involved.^[25] In the present study we report a different route to achieve hysteresis-free ferroelectric switching that is essentially independent of temperature and uses single-crystalline thin films of a classical ferroelectric BaTiO₃.

6.2 TEM imaging

Ferroelectric BaTiO₃ films are grown under low-strain on NdScO₃ substrates and display a well-understood domain structure and phase diagram.^[26,27] A detailed analysis of the local strain state across the film has been performed by transmission electron microscopy (TEM). A cross-sectional strain map of a thick (300 nm) film can be seen in **Figure 6.2a** and profiles extracted along the dotted arrows are shown in **Figure 6.2b,c**. The strain at the surface of the film corresponds to a so-called a/c domain pattern, that is alternating in-plane (a-domain) and out of plane (c-domain) polarized regions, common in tetragonal thin films. However, a strain gradient can be observed running across the thickness of the film. The strain difference between the two domain types gradually disappears towards the interface with the substrate, where the two domains are no longer distinguishable by strain analysis.

Thinner BaTiO₃ films crystallize in an ac*/bc* phase, derived from the well-known in-plane a/b

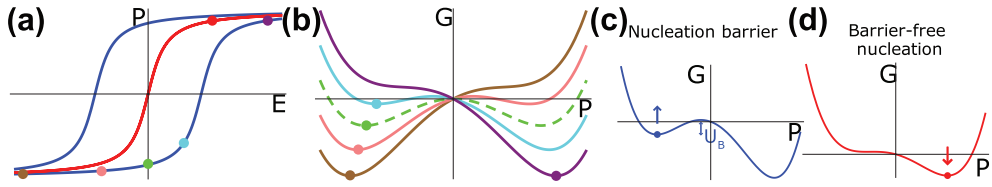


Figure 6.1 Intrinsic hysteresis in ferroelectrics. **a)** The sketch of a hysteresis loop in a typical ferroelectric during polarization switching under continuously varying the electric field, from the negative polarized state, under negative electric field, (brown and pink dots corresponding to the same color curves in **b**)) to the positive polarized state, under a positive electric field (purple dot and purple curve in **b**)). The green dot in **a**) corresponds to the symmetric free energy potential G (green curve in **b**)) with no applied field. Hysteresis originates by the tendency of the system to remain in the existing polarization state after reverting the applied electric field (light blue dot in **a**) and blue curve in **b**)) due to the presence of an energy barrier (U_B) for nucleation of the opposite polarization state **c**). An ideal hysteresis-free ferroelectric material, as sketched by the red curve in **a**), corresponds to an energy potential landscape with energy barriers smaller than $k_B T$, as for example the one in figure **d**).

phase (in-plane 90° domains), but with an additional small alternating c-polarization, designated by c_+^* or c_-^* .^[26] The cross-sectional TEM image of an 80 nm thick BaTiO₃ film (**Figure 6.2d**) reveals a domain wall inclination of 45° with respect to the substrate. Because the in-plane domain wall orientation is also 45° with respect to the top-view crystallographic axes, these data show that the domain walls for this ac_+^*/bc_-^* phase are parallel to (111) planes, different from the (110) domain wall plane that was predicted.^[27,28] The domain walls appear diffused in the TEM image due to their

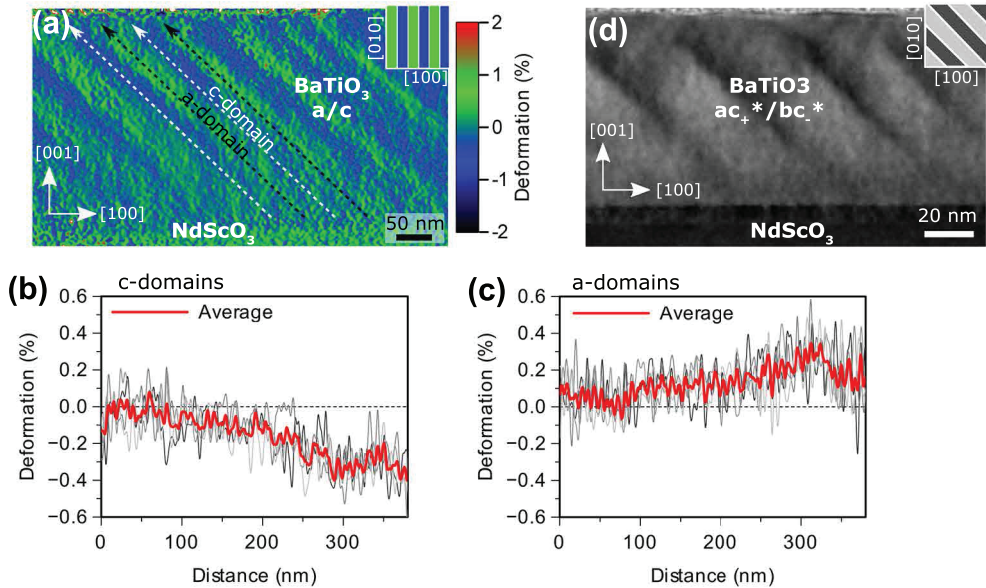


Figure 6.2 a) In-plane deformation map of a/c domains with (101) domain walls obtained by TEM (dark-field electron holography) in a 300 nm thick BaTiO₃ film. The inset in the top right corner illustrates the domain structure at the sample surface (viewed along the [001] direction). Due to the anisotropy of the substrate, only in-plane a-domains are found without the perpendicular b-domains (polarization along the b-axis). **b,c)** Deformation profiles extracted from map **a**) according to the dashed arrows in the c- and a-domains respectively. The strain is not uniform across the thickness of the film and there is a strain relaxation gradient. The lattice parameters near the interface in the a- and c-domains are almost equal, while at the surface they are distinctly different. **d)** TEM image of the ac_+^*/bc_-^* phase in an 80 nm thin film. The inset in the top right corner illustrates the domain structure at the sample surface (viewed along the [001] direction). The film has a phase transition from the ac_+^*/bc_-^* phase to the a/c phase for larger thicknesses at room temperature. These measurements have been performed by T. Denneulin, E. Snoeck and M. Hÿtch from CEMES-CNRS, Toulouse, France.

45° inclination with respect to the [010] measurement direction, which prevents high-resolution imaging of the strain state in this phase. However, the domain contrast is still higher near the surface than near the bottom interface, showing that a strain gradient is also present in this ac^*/bc^* phase.

Local TEM polarization mapping by CBED in the a/c phase (**Figure 6.3**) shows a polarization with tetragonal symmetry at the top surface and orthorhombic symmetry at the bottom interface, with the region in between too complex to figure out the polarization symmetry. A domain structure with alternating polarization is found for both symmetries.

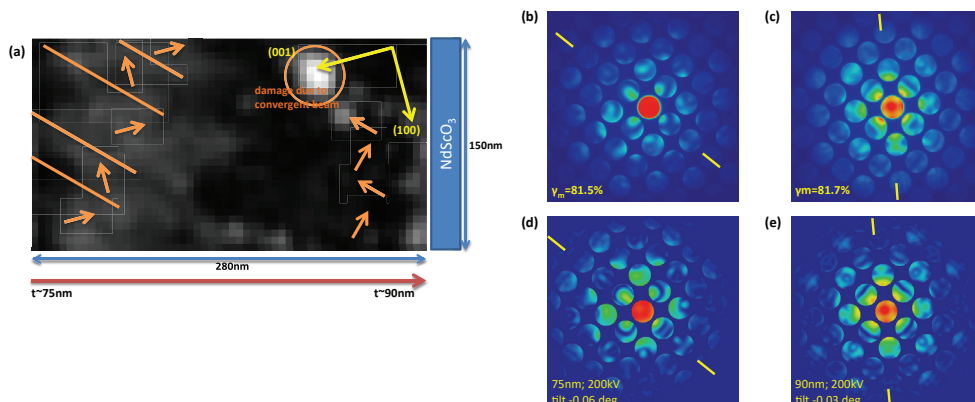


Figure 6.3 Polarization map of the BaTiO_3 thin film along [010] incidence. **a)** Shows the virtual annular dark-field (ADF) image reconstructed from the scanning convergent beam electron diffraction (CBED) dataset for a scanned region of $280\text{nm} \times 150\text{nm}$, integrating intensities from inner radius of 0.395 (1/\AA) to outer radius of 0.633 (1/\AA) . The orange arrows indicate the polarization directions, while the dashed lines indicate the domain boundaries. **b)** Representative CBED patterns showing the mirror plane directions along $\langle 100 \rangle$ near the surface of the film. **c)** Mirror-plane directions along $\langle 110 \rangle$ near the substrate. **d,e)** Simulated CBED patterns corresponding to (b,c), respectively. The orange circle indicate the damage caused by convergent electron probe. These measurements have been performed by Y.-T. Tsun and J.-M. Zuo from the University of Illinois, USA.

6.3 Ferroelectric hysteresis loops

A ‘slim’ ferroelectric hysteresis loop, with low coercive field, is measured on an out-of-plane capacitor structure of patterned top and continuous bottom SrRuO_3 electrodes (**Figure 6.4a**). The saturation polarization of $20\text{ }\mu\text{C}/\text{cm}^2$ (which includes some purely dielectric contributions) does not reach the bulk BaTiO_3 polarization of $27\text{ }\mu\text{C}/\text{cm}^2$ (the films are under low strain)^[29], which seems to point towards some non-switched polarization in the material. While it is hard to distinguish details in the ferroelectric loop itself, the displacement current obtained during the measurement shows two switching peaks, indicating that switching takes place in two steps (see for further details on double switching peak **Section 6.7**). The coercive field is found to be $5 \pm 2\text{ kV}/\text{cm}$. This is one order of magnitude smaller than in BaTiO_3 thin films with different domain structures, either on other^[29] or the same^[30] substrates.

These ferroelectric loop measurements (using large electric signals) can be compared to capacitance measurements (using smaller electrical signals) in **Figure 6.4b**. Those small-signal measurements address polarization due to reversible processes, such as intrinsic lattice shifts, excluding all extrinsic effects contributing to the switching.^[31] The coercive field is slightly smaller ($2\text{ kV}/\text{cm}$) while the polarization is nearly equal for both types of measurements. So it can then be concluded that nearly all polarization switches reversibly and there is essentially zero remanent polarization, in agreement with the large signal measurements.

The out-of-plane ferroelectric hysteresis loop decreases its coercive field when approaching

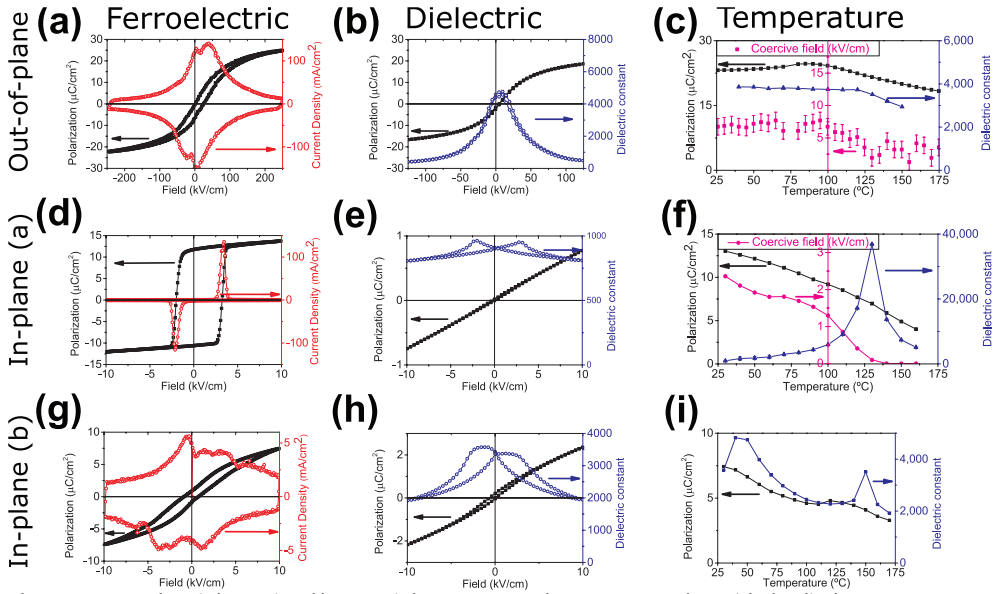


Figure 6.4 Ferroelectric large-signal hysteresis loops measured at 100 Hz together with the displacement switching current obtained from the ferroelectric hysteresis measurement at room temperature (a,d,g) and small-signal (or dielectric) measurements at 1 kHz giving the dielectric constant and the amount of reversible polarization from its integration (b,e,h). a,b) Out-of-plane direction, where the AC voltage in the dielectric measurement was 50 mV. Typical $\tan \delta$ loss values are 0.05 at the switching peak and 0.01 for the other fields. c) Large-signal polarization, coercive field and the maximum value of the dielectric constant obtained in the small-signal measurements at different temperatures for the out-of-plane direction. d,e) In-plane a-axis direction, where the AC voltage in the dielectric measurement is 100 mV. Typical $\tan \delta$ loss values are 0.03 at the switching peak and 0.005-0.01 for the other fields. f) Large-signal polarization, coercive field and the maximum value of the dielectric constant obtained in the small-signal measurements at different temperatures for the in-plane a-direction. g,h) In-plane b-axis direction, where the AC voltage in the dielectric measurement is 100 mV. Typical $\tan \delta$ loss values are 0.03 at the switching peak and 0.005-0.01 for the other fields. i) The large-signal polarization and the maximum value of the dielectric constant obtained in the small-signal measurements (the definition of the coercive field does not make much sense for the obtained ferroelectric hysteresis loops) at different temperatures for the in-plane b-direction.

the ferroelectric transition temperature T_c (called $T_{c,c}$ for this out-of-plane c-direction) at 130 °C, but the saturation polarization only slowly decreases its magnitude and remains far above this temperature (Figure 6.4c). The dielectric constant does not have a divergence at $T_{c,c}$ as expected, but it only decreases slowly with increasing temperature, with a slope change at $T_{c,c}$. This essentially temperature-independent dielectric constant of around 4000 is four times larger than predicted for these structures by Koukhar et al.^[27] and – to the best of our knowledge – larger than any of the temperature-independent dielectric constants reported for epitaxial thin films^[19,24,31,32].

Ferroelectric hysteresis loops were also measured along the a-axis in-plane direction (Figure 6.4d,e), where a polarization of 11 $\mu\text{C}/\text{cm}^2$ is obtained (with a single switching peak this time). This can be combined with the 20 $\mu\text{C}/\text{cm}^2$ for the out-of-plane loop which gives 31 $\mu\text{C}/\text{cm}^2$, a value comparable to the bulk polarization. One can explain this by considering two different surface areas which consist of in-plane or out-of-plane domains. Then the switching of the polarization proceeds, thus, via independently switching either only the out-of-plane or only the in-plane polarization. This in-plane ferroelectric hysteresis loop has a more standard temperature dependence (Figure 6.4f), with decreasing ferroelectric polarization, disappearance of the coercive field, and a low dielectric constant far away from $T_{c,a}$ coupled to a large divergence (up to 40,000) exactly at $T_{c,a}$.

The coercive field (E_c) along the in-plane a-direction ($E_{c,a}$) is only slightly smaller (3 kV/cm) than

along the out-of-plane ($E_{c,c}$) direction. The electric field full width at half maximum (FWHM) of the switching peak (E_{FWHM}), however, is below 1 kV/cm for this in-plane direction, significantly smaller than the 33 kV/cm measured for the out-of-plane direction. There is only little reversible small-signal polarization for this in-plane direction ($< 1 \mu\text{C}/\text{cm}^2$). Consequently, while the coercive field for the two measurement directions is similar, the amount of small-signal polarization and the FWHM of the switching peak are widely different. The remanence and the reversibility of the polarization are closely related to the FWHM of the switching peak and, thus, instead of the commonly used expression $\frac{1}{2}(E_c^+ - E_c^-)$, a better definition of hysteresis would be $\frac{1}{2}(E_c^+ - E_c^-)/E_{FWHM}$, where the hysteresis has a correction factor that takes the broadness of the switching peak into account.

The in-plane ferroelectric loops along the perpendicular (b-axis) in-plane direction (**Figure 6.4g,h**) reveal a complicated switching pattern (at room temperature) with multiple switching peaks, large FWHM and small switched polarization of only $7 \mu\text{C}/\text{cm}^2$. The temperature dependence (**Figure 6.4i**) reveals a $T_{c,b}$ of 50°C , the temperature where the static domain structure has a phase transition from the ac^*/bc^* to a/c phase. It is coupled to a broad divergence of the dielectric constant, resembling a broad transition range for the b-polarization to fully disappear. The large dielectric constant and rather large reversible polarization at room temperature is, thus, caused solely by its proximity to $T_{c,b}$.

The small parasitic polarization switching above 50°C (**Figure 6.5**) for the b-axis measurements can be explained by the design of these interdigitated electrodes (see also Figure 6.13). The observed coercive field for the switching along the b-axis is about three times larger than along the a-axis. The distance between the electrodes along the b-direction in this interdigitated structure is $5 \mu\text{m}$, and there is also a small parallel capacitor structure along the a-direction as well, which has a spacing of $15 \mu\text{m}$. So those parasitic switching peaks are arising from a-direction switching with a three times larger distance than the assumed b-electrode distance, giving an apparent coercive field that is three times larger.

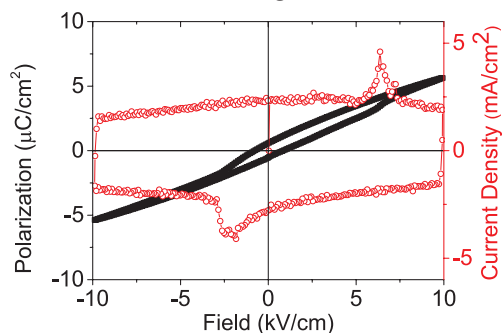


Figure 6.5 Ferroelectric hysteresis loop of the in-plane b-axis at 70°C .

In-plane measurements along the diagonal $\langle 110 \rangle$ directions give essentially the same switching behavior as the measurements along the a-direction. The type of switching peaks and the total polarization is equal to that a-direction; just the apparent coercive field along these $\langle 110 \rangle$ directions is $\sqrt{2}$ times larger than for the a-direction. If only the a-direction electric field is taken into account for these $\langle 110 \rangle$ electrodes, then the coercive field is equal to the coercive field found for the a-direction. So it means that for these $\langle 110 \rangle$ measurements, only the a-polarization is switched and the b-polarization remains passive. So this system is similar to ferromagnetic systems with a hard and soft magnetization direction.

6.4 Asymmetric hysteresis loops

Fully symmetric, relatively thick, electrodes (**Figure 6.6a**) give two, symmetric switching peaks. The corresponding piezoelectric deformation is symmetric and hysteresis-free, with an initial piezoelectric d_{33} coefficient of 70 pm/V , that decreases to 40 pm/V above an applied field of

125 kV/cm. These values are only slightly smaller than the 100 pm/V predicted for the *a/c* phase^[27] and they are high values for an epitaxial film that is subjected to substrate clamping^[33] (BaTiO₃ bulk *d*₃₃ coefficient is 100-125 pm/V^[34]), and comparable to those of freestanding BaTiO₃ films^[35] and to most PZT-based epitaxial thin films close to the Morphotropic Phase Boundary, which are reported in the range of 40-70 pm/V^[36,37]. Only good bulk materials and the best PZT thin films report higher piezoelectric activities (> 500 pm/V^[38] for bulk PZT and 200-300 pm/V^[13,39,40] for PZT thin films).

When symmetric thin electrodes were used (**Figure 6.6b**), no switching processes could be observed. They however do show a constant piezoelectric response of 40 pm/V which demonstrates that they still provide electrical contact. This non-switching behavior can be further investigated by pairing the electrodes asymmetrically with thick/thin electrodes, so that the two interfaces become dissimilar. That configuration then gives a hugely asymmetric ferroelectric and piezoelectric loop (**Figure 6.6c**). One of the two switching peaks disappears (see also **Section 6.8**), lowering the polarization at negative fields significantly. The piezoelectric response changes considerably and results in an almost perfect realization of the recently-proposed concept of a ‘strain diode’^[41], whereby the electromechanical response is large for positive fields (still the same 70 pm/V as for the symmetric electrodes) and largely suppressed for negative fields (to 20 pm/V). During the switching process, the piezoelectric activity is even increased to over 100 pm/V, comparable to non-epitaxial PZT films^[42], bulk single crystal BaTiO₃^[34] and the switching between different crystal symmetries in BiFeO₃^[43].

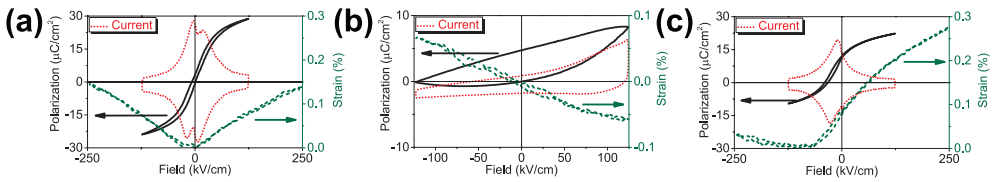


Figure 6.6 Ferroelectric loops together with their displacement currents and the piezoelectric deformation. **a)** Symmetric thick/thick electrode configuration (12 nm bottom and 20 nm top SrRuO₃ electrode). It has symmetric switching with low coercive field, and two sets of switching current peaks. **b)** Symmetric thin/thin electrode configuration (6 nm bottom and 6 nm top SrRuO₃ electrode). No clear ferroelectric switching is observed. **c)** Asymmetric thick/thin electrode configuration (6 nm bottom and 20 nm top SrRuO₃ electrode). Only a single set of switching current peaks is observed. The ferroelectric loop and piezoelectric deformation are highly asymmetric.

6.5 Discussion

We now turn to the discussion of the nature of the switching events. For this purpose we have performed *ab initio*-based effective Hamiltonian simulations, using the Hamiltonian given in Ref.^[44] and the parameters given in Ref.^[45]. For the small anisotropic strain^[26] the calculations yield various metastable domain configurations (**Figure 6.7a**) depending on the thermal history and the boundary conditions used. The *b*-axis ferroelectric switching below *T*_{C,*b*} gives normal ferroelectric switching between *a/b*⁺ and *a/b*⁻ phases, of which the polarization states are similar to the experimentally observed *ac*⁺/*bc*⁺ phases (**Figure 6.7b**). Above *T*_{C,*b*} in the *a/c* phase no clear ferroelectric switching is observed (**Figure 6.7c**), but significant reversible hysteresis-free polarization is induced by the electric field close to *T*_{C,*b*}, which explains the high dielectric constant found in the experiments. The polarization switching along the *a*-direction (**Figure 6.7d**) for the *a/c* initial state gives switching between *a/c*⁺ and *a/c*⁻ phases. The polarization switching along the *c*-direction (**Figure 6.7e**) is similar, with switching between *a/c*⁺ and *a/c*⁻ phases. The modelled coercive fields, while it is an overestimation (because it assumes a perfect, defect-free material^[10]), is lower in these epitaxial films than in the one modelled for free-standing BaTiO₃, and it correctly predicts that *E*_{C,*b*} < *E*_{C,*a*}, while not much can be said about *E*_{C,*c*} due to the large experimental error.

Both boundary conditions of the theoretical model do not allow for the strain gradients observed in the experiment (which are also not found for other BaTiO₃ thin films with conventional

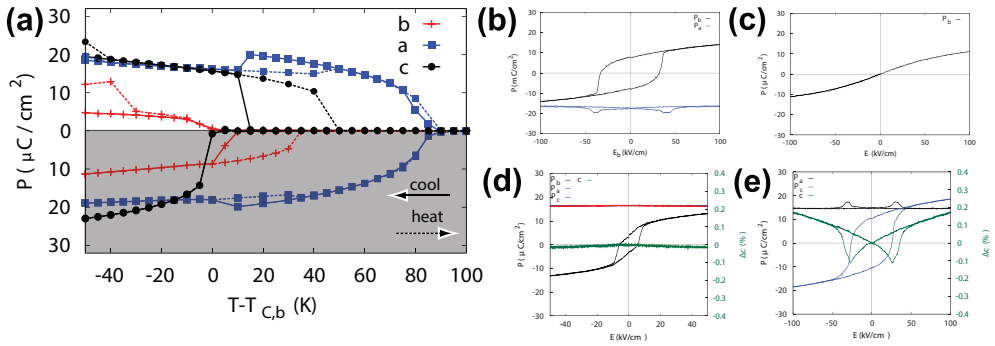


Figure 6.7 a) Phases found in cooling-down (solid lines) and heating-up (dashed lines) simulations for bulk-like (upper part, periodic boundary conditions) and thin-film like samples (lower part, double periodic boundary conditions). The temperature is given relative to the transition temperature $T_{C,b}$, experimentally found at 50 °C. Under periodic boundary conditions (double periodic boundary conditions) the following phases are found: paraelectric, a, a/c, ab^*/cb^* , ac/bc (paraelectric, a, a/b, ac/bc). In the simulations $T_{C,a} > T_{C,c}$ due to the fixed tensile in-plane strain and the underestimation of the thermal expansion in contrast to $T_{C,a} = T_{C,c}$ in experiment. b) Switching along the b-direction for the initial a/b phase found in double-periodic boundary conditions (below $T_{C,b}$). It switches between a/b+ and a/b- phases, with an intermediate ab monodomain phase which shows up in a single switching peak. c) Switching along the b-direction for an initial a/c phase found (above $T_{C,b}$), with only induced polarization. d) Switching along the a-direction for both the a/c and ab^*/cb^* (b^* is small b-polarization) phases is done between the a/c+ ($a-b^*/cb^*$) and a/c- ($a-b^*/cb^*$) phases through an intermediate ac monodomain phase. e) Switching along the out-of-plane c-direction for both the a/c and ab^*/cb^* phases (below $T_{C,c}$) is done between the a/c+ ($ab^*/c-b^*$) and a/c- ($ab^*/c-b^*$) phases through an intermediate ac monodomain phase. These calculations were performed by A. Grünebohm, University of Duisberg-Essen, Germany.

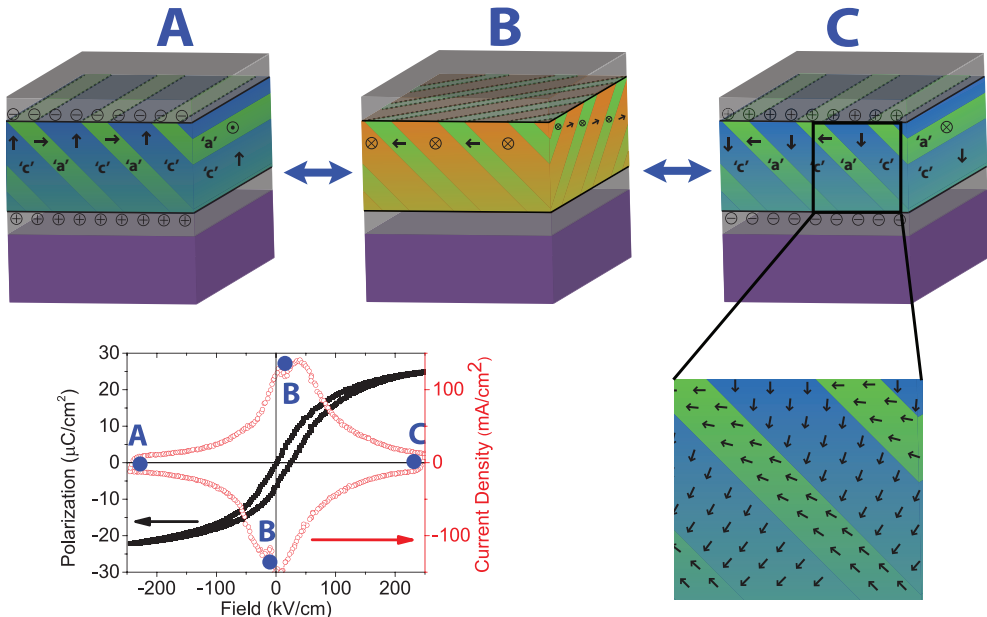


Figure 6.8 Proposed model for the out-of-plane ferroelectric switching. An a/c+ phase (A) at large negative fields is transformed, through an intermediate (mostly in-plane) ac^*/bc^* phase at zero field (for simplicity its parent a/b phase is drawn here), to an a/c phase at large positive fields (C). The labels 'a', 'b' and 'c' refer to the domain state at the top surface, as the polarization in those domains form a gradient from the top surface to the bottom interface, where at the bottom they form multidomain orthorhombic states. The color gradients represent the strain gradients that would be observed in TEM deformation mappings, with large differences at the top surface and an apparent single state at the bottom interface.

ferroelectric switching^[29,30]). Since it is well known that in ferroelectric perovskites the coupling between polarization and strain is strong, it is proposed that the polarization follows this strain gradient, and forms a bridging monoclinic domain with polarization that rotates from the $\langle 101 \rangle$ directions (compatible with a orthorhombic-like phases) at the bottom interface towards the $[100]$ and $[001]$ directions (tetragonal-like phases) at the top surface. BaTiO_3 at this strain state and temperature is predicted to be tetragonal, but the monoclinic and orthorhombic states are still close in energy^[26,27,46,47], they were for example already found in the calculated switching mechanism as an intermediate phase. The relative stability of these phases provides in this material a viable route to gradual strain relaxation. $\text{PbZr}_{1-x}\text{Ti}_x\text{O}_3$ -based materials do not have such a low-energy monoclinic and orthorhombic phase acting as a bridge between the two tetragonal directions. So there strain gradients, natural^[48] or compositional^[12], cannot induce such a polarization gradient.

The strain gradient observed in the BaTiO_3 films, will, by the nature of the flexoelectric effect, result in flexoelectric polarization. Such a phenomenon has been observed in PbTiO_3 thin films with a/c domains, where a flexoelectric polarization of $15 \mu\text{Ccm}^{-2}$ has been found, arising from a strain gradient of 0.75 mm^{-1} with a flexoelectric coefficient of 200 nC m^{-1} .^[48] The flexoelectric polarization induced by the material in Fig. 6.2a can be calculated in a similar manner. The out-of-plane strain changes from 0.3% to 0% (-0.3% to 0%) from the top surface to the bottom interface in the a -domains (c -domains), resulting in a strain gradient of $0.01 \mu\text{m}^{-1}$ in each domain. The intrinsic flexoelectric coefficient of BaTiO_3 has recently been determined to be 200 nC m^{-1} .^[49] In this material the calculated flexoelectric out-of-plane polarization would then be $0.2 \mu\text{Ccm}^{-2}$, which is a smaller value than the error in all of the ferroelectric measurements. Even if the strain would have relaxed in an 80 nm sample, the polarization would still be only $0.75 \mu\text{Ccm}^{-2}$. Horizontal strain gradients (like in the PbTiO_3 example^[48]) have not been measured in this material. So any flexoelectric effects arising due to the natural strain gradients will not make a significant impact on the results presented in this chapter.

This leads us to propose a modified switching pathway in **Figure 6.8**. A polarization gradient in the a/c phase goes from pure a/c at the top surface to an ac orthorhombic phase at the bottom interface. The broad switching peak with large reversible polarization and large dielectric constant is caused by a slow rotation of the polarization, aided by the naturally present polarization gradient and the naturally occurring monoclinic phases allowing polarization rotation^[50]. The double switching peak found in experiment is then proposed to be caused by the stabilization of an ac^*/bc^* intermediate bridging phase. This phase is already a monoclinic phase, acting as a natural bridge between the a/c phases. It is also structurally quite similar to the a/c phase, since the (101) walls of the a/c phase and the (111) walls of the ac^*/bc^* phase share the $[111]$ line, which provides plenty of nucleation points for the growth of new domains. When the field is removed, the depolarization effect gives a small driving force towards an in-plane polarized state, which can actually be reached due to the low energy cost to reach this available state by the rotation of the polarization and their mechanical similarity. This phase can also be stabilized by the asymmetric thick/thin electrodes, giving rise to the enhanced piezoresponse on the transition from the out-of-plane to the in-plane structure and low piezoresponse when that phase has been reached.

6.6 Conclusion

Concluding, this work demonstrates that it is possible to design ferroelectrics in which hysteresis-free polarization switching can be achieved without using dopants, in crystals with differently oriented phases close in energy. A microscopic analysis of the samples shows that there is gradual change in the domain structure from the bottom to the top interfaces, associated to a strain gradient. The coupling between strain and polarization in ferroelectrics suggests a continuum mechanism by which the polarization of the in-plane domains is found to gradually rotate to the out-of-plane direction, which gives rise to hysteresis-free ferroelectric loops and to a large essentially temperature-independent dielectric constant. In the same material it is also possible to get conventional ferroelectric hysteresis loops for the in-plane directions (which do not

have such a polarization gradient), and to change the transition temperature from a ferroelectric to a paraelectric-like state depending on the in-plane measurement direction, caused by the anisotropy of the substrate. This hysteresis-free direction, in turn, enables new energy-efficient electromechanical functionalities, such as the dielectric equivalent of a magnetic permalloy with high permittivity that is largely temperature-independent, or the additional possibility to build a strain diode. Similar mechanisms can be utilized in the design of other ferroelectrics and piezoelectrics, soft ferromagnets or energy-efficient shape-memory alloys.

6.7 Note on Double hysteresis loops

The reported double hysteresis loop with two switching peaks in the out-of-plane ferroelectric hysteresis loop has been assigned to a stable intermediate in-plane polarized phase. However, for a proper discussion, it is important to consider possible other origins of double hysteresis loops. Antiferroelectric interactions is one possible, although not often observed, origin of double hysteresis loops, for example observed in electric-field induced polarization in BaTiO₃ single crystals slightly above the Curie temperature, which are stable for a limited temperature range.^[23] The most common double hysteresis loops are so-called pinched or constricted loops.^[25,51–53] They arise because locally some areas of the material have an internally stabilized pinned polarization, which on the macroscopic scale forms regions with a polarization that is opposite to the other regions. This mechanism is most common in ceramic materials, but also in thin films this is sometimes seen. These pinched loops have to disappear after the material has been cycled with large AC fields for long times, where higher temperatures makes this process go faster. This process is called de-aging. This cycling will remove the local pinning of the dipoles, after which only a single hysteresis loop remains.

These mechanisms have in common that the intermediate states have a macroscopic anti-parallel polarization, and the transition between the intermediate and final states only concerns non-elastic out-of-plane polarization. The out-of-plane ferroelectric hysteresis loops in this chapter can thus not result from these mechanisms, since an enhanced piezoelectric activity is found during the switching to the intermediate phase (for the asymmetric thick/thin bottom electrodes). So for those out-of-plane ferroelectric loops, a 90° domain rotation with associated elastic changes is observed. Furthermore, the double ferroelectric hysteresis loop is stable under cycling under large AC fields for any amount of (experimentally accessed) time, at all temperatures below $T_{C,c}$. If the origin of the double hysteresis loop were pinched loops, then the two switching peaks should have changed over the AC field cycling. Somewhat related phenomena have been observed in successive 90° domain wall switching giving rise to two separate switching events^[54]; such successive 90° switching events happening at a single field in one switching peak^[11]; or single 90° domain switching^[55].

The in-plane ferroelectric loops however do show more of pinched loop behavior. The a-axis hysteresis loop changes after 10⁶ cycles with a large AC field. The progression of the ferroelectric hysteresis loop with field cycles can be seen in **Figure 6.9**. Before any cycling, the ferroelectric hysteresis loop is very small and hardly any switching is observed. After a few cycles, this is transformed into an unstable double hysteresis loop, where the two switching peaks slowly merge into a single peak after cycling for some time. A short increase of temperature, or letting the system rest for a few minutes, will however age the material into two switching peaks, which can be de-aged in a similar manner. The physical origin of the aging is not known exactly, since normal pinched ferroelectrics do not usually age within minutes or age by increasing the temperature. It is not impossible that the low hysteresis of the out-of-plane direction helps to age the sample much faster than normal ferroelectrics, by providing a low-energy pathway to change the polarization.

The de-aging for the ferroelectric hysteresis loop along the in-plane b-direction takes much longer as seen in **Figure 6.10**, using the same AC field type. The virgin ferroelectric hysteresis loop has two switching peaks, together with some built-in field. After 10⁸ cycles the switching peaks have

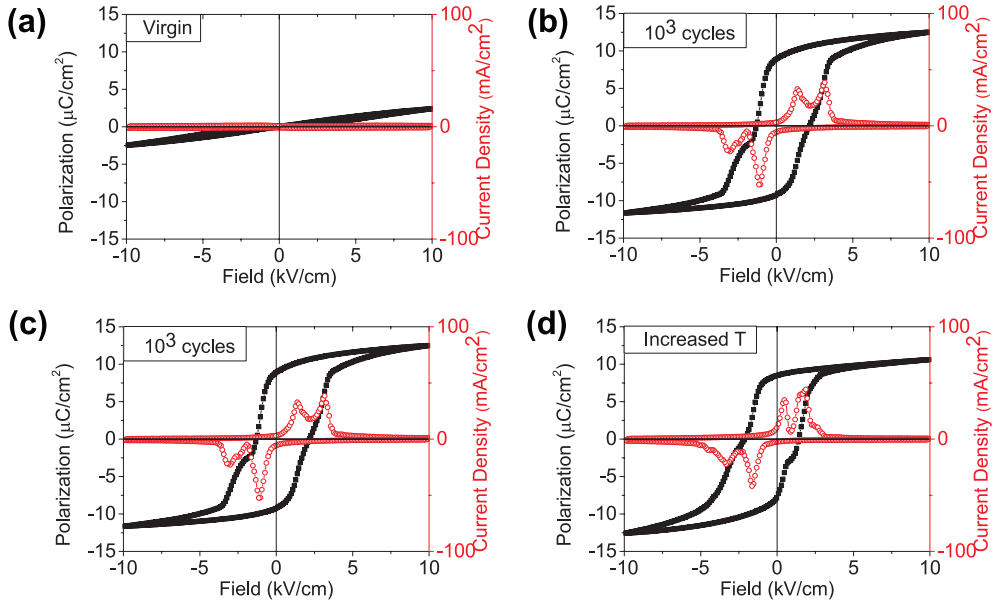


Figure 6.9 In-plane ferroelectric hysteresis loop along the *a*-direction after AC field cycling at 30 °C at 10 kV/cm with a frequency of 1kHz-100kHz. **a)** Ferroelectric hysteresis loop in the virgin state, before any cycling, after cooling down slowly from 150 °C. **b)** Ferroelectric hysteresis loop after 10^3 cycles. **c)** Ferroelectric hysteresis loop after 10^6 cycles. **d)** The ferroelectric hysteresis loop measured after the temperature was increased by 5°C, right after the measurement of (c).

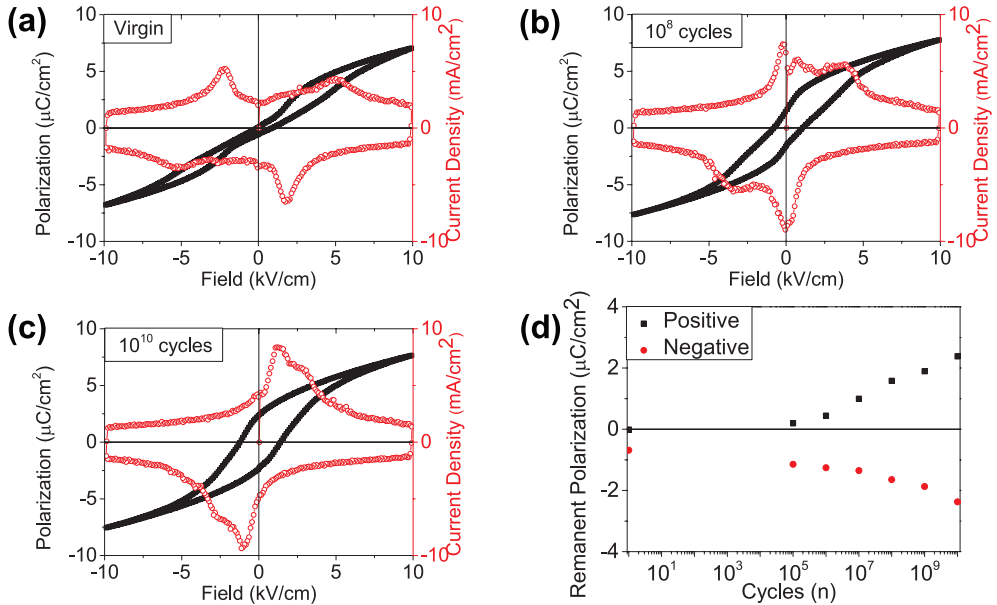


Figure 6.10 In-plane ferroelectric hysteresis loop along the *b*-direction after AC field cycling at 10 kV/cm with a frequency of 1kHz-100kHz. **a)** Ferroelectric hysteresis loop in the virgin state, before any cycling. **b)** Ferroelectric hysteresis loop after 10^8 cycles. **c)** Ferroelectric hysteresis loop after 10^{10} cycles. **d)** Fatigue measurement, giving the value of the remanent polarization as a function of field cycles.

started to merge, but are still clearly visible as different switching peaks. The built-in field is also slowly being cancelled. Even after 10^{10} cycles (AC field applied for more than a day!), there are still traces visible from the original switching peaks. If the origin of the pinched loops here had been equal to the case of the a-axis ferroelectric loops, then the de-aging should have taken place at a similar amount of field cycles. This increased de-aging difficulty is then probably caused by the large number of (meta-)stable phases observed below $T_{c,b}$. From the other directions of the switching loops it can be seen that the a/c phase can be stabilized by an electric field, on which the theoretically found ab^*/cb^* and a/b phases can be added as (meta-)stable phases. The a/c phase will contribute with a large dielectric constant and a very broad switching peak at 0 kV/cm and the ab^*/cb^* phase can contribute as shown in **Figure 6.11**. It takes many field cycles to remove those two phases and revert to the more favorable a/b switching (since it allows for the largest b-polarization). It will also take many cycles due to the proximity of the $T_{c,b}$ phase transition, which further stabilizes the a/c phases even at room temperature.

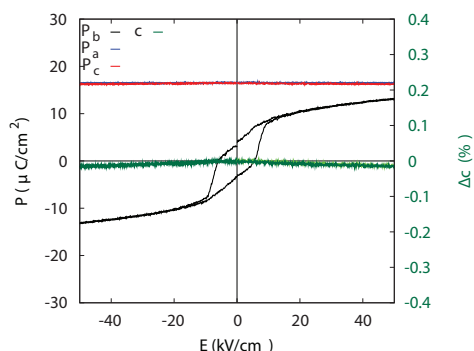


Figure 6.11 Theoretical ferroelectric hysteresis loop starting from an initial ab^*/cb^* phase. The switching takes place between the ab^*/cb^* and ab^*/cb^* phases. The a/c part of this domain pattern remains essentially unchanged during switching. These calculations were performed by A. Grünebohm, University of Duisburg-Essen, Germany.

6.8 Note on top-top ferroelectric measurements on symmetric/asymmetric electrodes

Further proof of the polarization blocking for different electrodes can be gathered by looking at top-top measurements for the symmetric and asymmetric electrodes. Top-top measurements can be seen as two top-bottom measurements back-to-back, so two capacitor structures, with the original top electrode on both surfaces, and the original bottom electrode in the middle.

The top-top measurements for the thick/thin electrodes in **Figure 6.12a** show a greatly reduced and fully symmetric polarization. Since these two capacitors are positioned back-to-back, while switching, one of the two capacitor structures will try to align the polarization towards the thin bottom electrode, and the other will try to align it away from this thin bottom electrode. Since only one of the out-of-plane polarization is possible in this electrode configurations, the switching is always blocked, so in principle it should not be able for this top-top capacitor structure to give any switching. However, the broadness of the switching peak, which propagates to both positive and negative fields, makes sure there is still some possible switching remaining, rather than the otherwise expected zero polarization switching.

The top-top measurements for the thick/thick electrodes (**Figure 6.12b**) shows that the polarization is only slightly smaller than for the top-bottom measurements. The polarization should have been exactly equal to the top-bottom measurement, but the not yet perfectly thick electrode decreases the polarization slightly. The two switching peaks seen for the individual top-bottom measurements are not exactly equal in magnitude, so even in these relatively thick electrodes, one of the out-of-plane polarizations will still be partially blocked. Different areas of the sample have small differences in how much polarization is blocked, with up to 20 % differences. An even thicker bottom electrode (paired with a similar top electrode) should make the switching fully symmetric, but thicker electrodes will give some strain relaxation, because the critical thickness for $SrRuO_3$

on this substrate (under 2 % tensile strain) is rather low. The BaTiO₃ material deposited on top will then not be under the correct epitaxial strain to obtain the same type of ferroelectric loop.

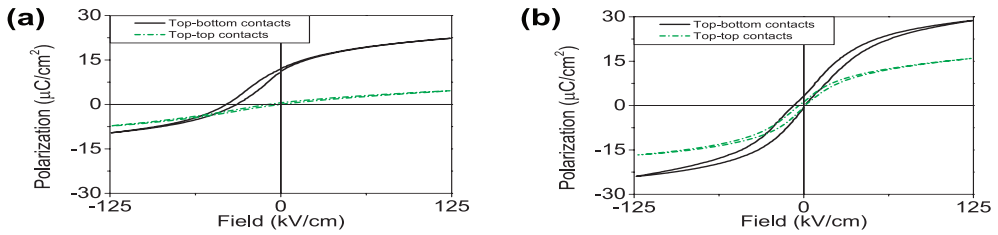


Figure 6.12 Measurements for *c*-direction top-top and top-bottom electrodes on thick/thin (20/6 nm) top/bottom electrodes (a) and thick/thick (20/12 nm) top/bottom electrodes (b).

6.9 Experimental

Thin foils for TEM measurements were prepared using a focused ion beam and a scanning electron microscope (FIB-SEM) FEI Helios. The final milling was carried out at 8 kV and the lamella thickness was in the 100-200 nm range. Dark-field electron holography^[56] was carried out using a Hitachi HF-3300 transmission electron microscope (I2TEM-Toulouse) equipped with a cold-field emission gun operated at 300 kV, two specimen stages (the standard stage within the pole piece gap of the objective lens and an upper stage placed above the objective lens), an image corrector (CEOS B-COR for correcting off-axis aberrations), four electron biprisms and a 4k×4k camera (Oneview Gatan).

The sample was inserted in the upper stage to obtain a large holographic field-of-view. The sample was oriented a few degrees out of zone-axis to increase the intensity of a diffracted beam (two-beam condition). The incident beam was tilted to bring the diffracted beam onto the optical axis and a small objective aperture was inserted. A double biprism configuration was used to obtain holograms without Fresnel fringes. The fringe spacing was 2 nm and the hologram width was 400 nm. The holograms were treated using the Holodark plug-in software (HREM Research Inc.) for Digital Micrograph (Gatan). Phase images were reconstructed using a half-cosine mask in Fourier space. The spatial resolution in the strain map is 6 nm and the precision is 0.1 %.

Patterning of the top electrodes was done using an etch mask on a homogeneous SrRuO₃ top electrode (deposited at 700 °C). Ferroelectric measurements have been performed on a commercial aixACCT TFA2000 system (applying positive field to the top electrode), applying triangular voltage pulses of varying frequency, measuring using a virtual ground method. The piezoelectric deformation has been measured on a commercial aixACCT Double Beam Laser Interferometer (DBLI), where a laser is reflected off a Pt top electrode (deposited on top of the SrRuO₃ electrode), and then off the bottom of the substrate, polished and covered homogeneously with Pt, and then combined with a reference beam to measure the interference pattern.



Figure 6.13 Interdigitated electrodes for in-plane measurements. The red area is where the electrodes are located. The distance between the electrodes is 5 mm; the distance between the large electrode areas is 215 mm; the length where the interdigitated electrodes run parallel is 185 mm; and the distance between the tip of the interdigitated electrodes and the big electrode area is 15 mm. The number of electrodes varies between 16 and 57. Another design with a 115 mm length of the electrodes gave comparable results.

These structures have been developed by S. Matzen, Université Paris-Sud, France.

The ferroelectric and piezoelectric measurements did not depend on the electrode size (which varied between lateral dimensions of 10 to 200 μm) and unless leakage was observed, the results were consistent across all those measurement pads and grown samples. The measurement frequency did not change the intrinsic switching between 0.01 Hz and 5 kHz (which are the limits of the measurement setup). Extrinsic effects did affect the measurements: the low frequency measurements had problems with leakage and the high frequency measurements did not allow for fast enough discharging of the capacitor^[57] (too large RC time constant), so the measurements presented were performed at 100 Hz, as a compromise between those two extrinsic effects.

The capacitor structure design for the in-plane ferroelectric measurements are interdigitated electrodes with dimensions as given in **Figure 6.13**. The distance between the electrodes is 5 mm, while the length of the parallel electrodes is 185 μm . The electrode capacitor area was assumed to be the length of the electrode multiplied by the film thickness, thereby ignoring any inhomogeneous electric fields and contributions from the substrate and air. Since the distance between the electrodes is 50 times larger than the film thickness, inhomogeneous electric fields will likely not give large contributions. However, it is not completely correct to ignore the substrate contributions (dielectric constant of 20)^[58], or the role of anisotropic strain on the dielectric constant in the different directions (which can give changes of up to 20 %)^[59]. So the dielectric constants and the polarization values obtained from the measurements should be taken with a 20-30 % error. But since the different effects reported for the three different orientations of the electric field are much larger than those errors, they can still be considered as a significant result.

The in-plane dielectric measurements were performed at an AC voltage of 100 mV, which corresponds to a field of 0.2 kV/cm. The out-of-plane dielectric measurements shown in the paper were obtained at an AC voltage of 50 mV, which corresponds to an electric field of 6.25 kV/cm. To get a fair comparison between the dielectric measurements in both structures, the electric field in both measurements should be equal. A reduction of the AC field in the out-of-plane direction to 2 mV (corresponding to 0.25 kV/cm) did not give any significant changes in the properties and conclusions. Only an increase of noise was observed, which was why the lower noise figures at 50 mV are presented in the paper. A reduction to 1 mV AC field increased the noise to such a high level that no meaningful conclusions could be drawn.

For the theoretical calculations the feram code was used, which is based on the effective Hamiltonian discussed in Ref.^[44] and the parametrization given in Ref.^[45]. The molecular dynamics simulations were performed in the NPT ensemble, employing a Nosé-Poincaré thermostat, periodic boundary conditions, and a simulation box of $96 \times 96 \times 96$ unit cells. An ideal bulk material is modeled, without surfaces and depolarizing fields. To simulate the effect of epitaxial strain, the elements η_1 and η_2 of the homogeneous strain tensor (in standard Voigt notation) are fixed to the external strain η , and η_6 is set to zero, see Ref.^[47]. The system is thermalized at a given temperature above T_c (or well below the lowest T_c) and cooled down (or heated up) in temperature steps of 10 K. In addition, cooling-down simulations have been performed for a short-circuited film of 48 unit cells thickness and ideal electrodes applying double-periodic boundary conditions^[44]. Starting with the thermalized configurations, the electrical field is ramped on and off with a rate of 0.002 kV/fs and the change of polarization and strain along c are recorded every 100th field step.

6.10 References

- [1] M. E. Lines and A. M. Glass. “*Principles and Applications of Ferroelectrics and Related Materials.*” Oxford University Press (1977)
- [2] D. B. Strukov, G. S. Snider, D. R. Stewart and R. S. Williams. “The missing memristor found.” *Nature* **453**, 80–83 (2008)
- [3] J. F. Scott. “*Ferroelectric Memories.*” Springer-Verlag Berlin Heidelberg (2000)
- [4] A. S. Mischenko, Q. Zhang, J. F. Scott, R. W. Whatmore and N. D. Mathur. “Giant Electrocaloric Effect in Thin-Film $\text{PbZr}_{0.95}\text{Tio}_{0.05}\text{O}_3$.” *Science* **311**, 1270–1271 (2006)

- [5] J. Liu, T. Gottschall, K. P. Skokov, J. D. Moore and O. Gutfleisch. "Giant magnetocaloric effect driven by structural transitions." *Nature materials* **11**, 620–626 (2012)
- [6] B. Chu, X. Zhou, K. Ren, B. Neese, M. Lin, Q. Wang, F. Bauer and Q. M. Zhang. "A Dielectric Polymer with High Electric Energy Density and Fast Discharge Speed." *Science* **313**, 334–336 (2006)
- [7] C. Ru, L. Chen, B. Shao, W. Rong and L. Sun. "A hysteresis compensation method of piezoelectric actuator: Model, identification and control." *Control Engineering Practice* **17**, 1107–1114 (2009)
- [8] L. Néel, R. Pauthenet, G. Rimet and V. S. Giron. "On the Laws of Magnetization of Ferromagnetic Single Crystals and Polycrystals. Application to Uniaxial Compounds." *Journal of Applied Physics* **27**, (1960)
- [9] S. Fähler, U. K. Rößler, O. Kastner, J. Eckert, G. Eggeler, H. Emmerich, P. Entel, S. Müller, E. Quandt and K. Albe. "Caloric effects in ferroic materials: New concepts for cooling." *Advanced Engineering Materials* **14**, 10–19 (2012)
- [10] S. Liu, I. Grinberg and A. M. Rappe. "Intrinsic ferroelectric switching from first principles." *Nature* **534**, 360–363 (2016)
- [11] R. Xu, S. Liu, I. Grinberg, J. Karthik, A. R. Damodaran, A. M. Rappe and L. W. Martin. "Ferroelectric polarization reversal via successive ferroelastic transitions." *Nature materials* **14**, 79–86 (2014)
- [12] J. C. Agar, A. R. Damodaran, M. B. Okatan, J. Kacher, C. Gammer, R. K. Vasudevan, S. Pandya, R. V. K. Mangalam, G. A. Velarde, S. Jesse, N. Balke, A. M. Minor, S. V. Kalinin and L. W. Martin. "Highly-mobile ferroelastic domain walls in compositionally-graded ferroelectric thin films." *Nature Materials* **15**, 549–556 (2016)
- [13] V. Nagarajan, A. Roytburd, A. Stanishevsky, S. Prasertchoung, T. Zhao, L. Chen, J. Melngailis, O. Auciello and R. Ramesh. "Dynamics of ferroelastic domains in ferroelectric thin films." *Nature materials* **2**, 43–47 (2003)
- [14] B. Ezraty, A. Vergnes, M. Banzhaf, Y. Duverger, A. Huguenot, A. R. Brochado, S. Su, L. Espinosa, L. Loiseau, B. Py, A. Typas and F. Barras. "Domain Dynamics During Ferroelectric Switching." *Science* **334**, 968–971 (2011)
- [15] P. Gao, J. Britson, J. R. Jokisaari, C. T. Nelson, S.-H. Baek, Y. Wang, C.-B. Eom, L.-Q. Chen and X. Pan. "Atomic-scale mechanisms of ferroelastic domain-wall-mediated ferroelectric switching." *Nature communications* **4**, 2791 (2013)
- [16] C. S. Ganpule, V. Nagarajan, B. K. Hill, A. L. Roytburd, E. D. Williams, R. Ramesh, S. P. Alpay, A. Roelofs, R. Waser and L. M. Eng. "Imaging three-dimensional polarization in epitaxial polydomain ferroelectric thin films." *Journal of Applied Physics* **91**, 1477 (2002)
- [17] R. J. Zeches, M. D. Rossell, J. X. Zhang, A. J. Hatt, Q. He, C.-H. Yang, A. Kumar, C. H. Wang, A. Melville, C. Adamo, G. Sheng, Y.-H. Chu, J. F. Ihlefeld, R. Erni, C. Ederer, V. Gopalan, L. Q. Chen, D. G. Schlom, N. A. Spaldin, L. W. Martin and R. Ramesh. "A strain-driven morphotropic phase boundary in BiFeO_3 ." *Science* **326**, 977–980 (2009)
- [18] F. Weyland, M. Acosta, J. Koruza, P. Breckner, J. Rödel and N. Novak. "Criticality: Concept to Enhance the Piezoelectric and Electrocaloric Properties of Ferroelectrics." *Advanced Functional Materials* (2016)
- [19] S. H. Baek, J. Park, D. M. Kim, V. A. Aksyuk, R. R. Das, S. D. Bu, D. A. Felker, J. Lettieri, V. Vaithyanathan, S. S. N. Bharadwaja, N. Bassiri-Gharb, Y. B. Chen, H. P. Sun, C. M. Folkman, H. W. Jang, D. J. Kreft, S. K. Streiffer, R. Ramesh, X. Q. Pan, S. Trolier-McKinstry, D. G. Schlom, M. S. Rzchowski, R. H. Blick and C. B. Eom. "Giant Piezoelectricity on Si for Hyperactive MEMS." *Science* **334**, 958–961 (2011)
- [20] Z. Luo, D. Zhang, Y. Liu, D. Zhou, Y. Yao, C. Liu, B. Dkhil, X. Ren and X. Lou. "Enhanced electrocaloric effect in lead-free $\text{BaTi}_{1-x}\text{Sn}_x\text{O}_3$ ceramics near room temperature." *Applied Physics Letters* **105**, 102904 (2014)
- [21] P. Wu, X. Ma, Y. Li, C.-B. Eom, D. G. Schlom, V. Gopalan and L.-Q. Chen. "Influence of interfacial coherency on ferroelectric switching of superlattice $\text{BaTiO}_3/\text{SrTiO}_3$." *Applied Physics Letters* **107**, 122906 (2015)
- [22] L. Hong, P. Wu, Y. Li, V. Gopalan, C. B. Eom, D. G. Schlom and L. Q. Chen. "Piezoelectric enhancement of $(\text{PbTiO}_3)_m/(\text{BaTiO}_3)_n$ ferroelectric superlattices through domain engineering." *Physical Review B* **90**, 174111 (2014)
- [23] W. J. Merz. "Double Hysteresis Loop of BaTiO_3 at the Curie Point." *Physical Review* **91**, 513–517 (1953)
- [24] P. Zubko, N. Jecklin, N. Stucki, C. Lichtensteiger, G. Rispens and J.-M. Triscone. "Ferroelectric Domains in $\text{PbTiO}_3/\text{SrTiO}_3$ Superlattices." *Ferroelectrics* **433**, 127–137 (2012)

- [25] D. Damjanovic. "Hysteresis in Piezoelectric and Ferroelectric Materials" in *The Science of Hysteresis*, Elsevier Inc. (2005)
- [26] A. S. Everhardt, S. Matzen, N. Domingo, G. Catalan and B. Noheda. "Ferroelectric Domain Structures in Low-Strain BaTiO₃." *Advanced Electronic Materials* **2**, 1500214 (2015)
- [27] V. G. Koukhar, N. A. Pertsev and R. Waser. "Thermodynamic theory of epitaxial ferroelectric thin films with dense domain structures." *Physical Review B* **64**, 214103 (2001)
- [28] P. Marton, I. Rychetsky and J. Hlinka. "Domain walls of ferroelectric BaTiO₃ within the Ginzburg-Landau-Devonshire phenomenological model." *Physical Review B* **81**, 144125 (2010)
- [29] K. J. Choi, M. Biegalski, Y. L. Li, A. Sharan, J. Schubert, R. Uecker, P. Reiche, Y. B. Chen, X. Q. Pan, V. Gopalan, L.-Q. Chen, D. G. Schlom and C. B. Eom. "Enhancement of ferroelectricity in strained BaTiO₃ thin films." *Science* **306**, 1005–1009 (2004)
- [30] A. R. Damodaran, E. Breckenfeld, Z. Chen, S. Lee and L. W. Martin. "Enhancement of Ferroelectric Curie Temperature in BaTiO₃ Films via Strain-Induced Defect Dipole Alignment." *Advanced Materials* **26**, 6341–6347 (2014)
- [31] P. Gerber, C. K ugeler, U. B ottger and R. Waser. "Effects of reversible and irreversible ferroelectric switchings on the piezoelectric large-signal response of lead zirconate titanate thin films." *Journal of Applied Physics* **98**, 124101 (2005)
- [32] J. H. Haeni, P. Irvin, W. Chang, R. Uecker, P. Reiche, Y. L. Li, S. Choudhury, W. Tian, M. E. Hawley, B. Craigo, A. K. Tagantsev, X. Q. Pan, S. K. Streiffer, L. Q. Chen, S. W. Kirchoefer, J. Levy and D. G. Schlom. "Room-temperature ferroelectricity in strained SrTiO₃." *Nature* **430**, 758–761 (2004)
- [33] R. Mahjoub, S. P. Alpay and V. Nagarajan. "Theory of giant electromechanical response from ferroelectric bilayers with polydomain structures due to interlayer and interdomain coupling." *Physical Review Letters* **105**, 1–4 (2010)
- [34] S. W. Ada, S. S. Uzuki, T. N. Oma, T. S. Uzuki and M. O. Sada. "Enhanced Piezoelectric Property of Barium Titanate Single Crystals with Engineered Domain Configurations." *Japanese Journal of Applied Physics* **38**, 5505 (1999)
- [35] K.-I. Park, S. Xu, Y. Liu, G. T. Hwang, S.-J. L. Kang, Z. L. Wang and K. J. Lee. "Piezoelectric BaTiO₃ thin film nanogenerator on plastic substrates." *Nano Letters* **10**, 4939–4943 (2010)
- [36] A. Kholkin, M. Calzada, P. Ramos, J. Mendiola and N. Setter. "Piezoelectric properties of Ca-modified PbTiO₃ thin films." *Applied Physics Letters* **69**, 3602–3604 (1996)
- [37] M. Boota, E. P. Houwman, M. Dekkers, M. D. Nguyen, K. H. Vergeer, G. Lanzara, G. Koster and G. Rijnders. "Properties of epitaxial, (001)- and (110)-oriented (PbMg_{1/3}Nb_{2/3}O₃)_{2/3}-(PbTiO₃)_{1/3} films on silicon described by polarization rotation." *Science and Technology of Advanced Materials* **17**, 45–57 (2016)
- [38] B. Jaffe, J. W. J. Crook and H. L. Jaffe. "Piezoelectric Ceramics." Academic Press (1971)
- [39] S.-H. Baek, M. S. Rzchowski and V. A. Aksyuk. "Giant piezoelectricity in PMN-PT thin films: Beyond PZT." *MRS Bulletin* **37**, 1022–1029 (2012)
- [40] G. Liu, Q. Zhang, H.-H. Huang, P. Munroe, V. Nagarajan, H. Simons, Z. Hong and L.-Q. Chen. "Reversible Polarization Rotation in Epitaxial Ferroelectric Bilayers." *Advanced Materials Interfaces* **3**, 1600444 (2016)
- [41] U. K. Bhaskar, N. Banerjee, A. Abdollahi, G. Rijnders, E. Solanas and G. Catalan. "Flexoelectric MEMS: towards an electromechanical strain diode." *Nanoscale* **8**, 1293–1298 (2016)
- [42] P. Gerber, U. B ottger and R. Waser. "Composition influences on the electrical and electromechanical properties of lead zirconate titanate thin films." *Journal of Applied Physics* **100**, 124105 (2006)
- [43] J. X. Zhang, B. Xiang, Q. He, J. Seidel, R. J. Zeches, P. Yu, S. Y. Yang, C. H. Wang, Y.-H. Chu, L. W. Martin, A. M. Minor and R. Ramesh. "Large field-induced strains in a lead-free piezoelectric material." *Nature nanotechnology* **6**, 98–102 (2011)
- [44] T. Nishimatsu, U. V. Waghmare, Y. Kawazoe and D. Vanderbilt. "Fast molecular-dynamics simulation for ferroelectric thin-film capacitors using a first-principles effective Hamiltonian." *Physical Review B* **78**, 104104 (2008)
- [45] T. Nishimatsu, M. Iwamoto, Y. Kawazoe and U. V. Waghmare. "First-principles accurate total energy surfaces for polar structural distortions of BaTiO₃, PbTiO₃, and SrTiO₃: Consequences for structural transition temperatures." *Physical Review B* **82**, 134106 (2010)
- [46] Y. L. Li and L. Q. Chen. "Temperature-strain phase diagram for BaTiO₃ thin films." *Applied Physics Letters* **88**, 72905 (2006)
- [47] A. Gr unebohm, M. Marathe and C. Ederer. "Ab initio phase diagram of BaTiO₃ under epitaxial strain

- revisited." *Applied Physics Letters* **107**, 102901 (2015)
- [48] G. Catalan, A. Lubk, A. H. G. Vlooswijk, E. Snoeck, C. Magen, A. Janssens, G. Rispens, G. Rijnders, D. H. A. Blank and B. Noheda. "Flexoelectric rotation of polarization in ferroelectric thin films." *Nature materials* **10**, 963–967 (2011)
- [49] J. Narvaez, S. Saremi, J. Hong, M. Stengel and G. Catalan. "Large Flexoelectric Anisotropy in Paraelectric Barium Titanate." *Physical Review Letters* **115**, 37601 (2015)
- [50] L. Bellaiche, A. García and D. Vanderbilt. "Finite-Temperature Properties of $\text{Pb}(\text{Zr}_{1-x}\text{Ti}_x)\text{O}_3$ Alloys from First Principles." *Physical Review Letters* **84**, 5427–5430 (2000)
- [51] K. Carl and K. H. Hardtl. "Electrical after-effects in $\text{Pb}(\text{Ti,Zr})\text{O}_3$ ceramics." *Ferroelectrics* **17**, 473–486 (1978)
- [52] M. I. Morozov and D. Damjanovic. "Hardening-softening transition in Fe-doped $\text{Pb}(\text{Zr,Ti})\text{O}_3$ ceramics and evolution of the third harmonic of the polarization response." *Journal of Applied Physics* **104**, 34107 (2008)
- [53] P. Erhart, P. Träskelin and K. Albe. "Formation and switching of defect dipoles in acceptor-doped lead titanate: A kinetic model based on first-principles calculations." *Physical Review B* **88**, 24107 (2013)
- [54] N. Bar-Chaim, M. Brunstein, J. Grünberg and A. Seidman. "Electric field dependence of the dielectric constant of PZT ferroelectric ceramics." *Journal of Applied Physics* **45**, 2398–2405 (1974)
- [55] A. I. Khan, X. Marti, C. Serrao, R. Ramesh and S. Salahuddin. "Voltage-Controlled Ferroelastic Switching in $\text{Pb}(\text{Zr}_{0.2}\text{Ti}_{0.8})\text{O}_3$ Thin Films." *Nano Letters* **15**, 2229–2234 (2015)
- [56] M. Hÿtch, F. Houdellier, F. Hÿe and E. Snoeck. "Nanoscale holographic interferometry for strain measurements in electronic devices." *Nature* **453**, 1086–1089 (2008)
- [57] I. Fina. "Ferroelectricity and magnetoelectric coupling in magnetic ferroelectrics and artificial multiferroic heterostructures." PhD Thesis Universitat de Barcelona (2012)
- [58] H. M. Christen, G. E. Jellison Jr., I. Ohkubo, S. Huang, M. E. Reeves, E. Cicerrella, J. L. Freeouf, Y. Jia and D. G. Schlom. "Dielectric and optical properties of epitaxial rare-earth scandate films and their crystallization behavior." *Applied Physics Letters* **88**, 262906 (2006)
- [59] Y. Lin, X. Chen, S. W. Liu, C. L. Chen, J. S. Lee, Y. Li, Q. X. Jia and A. Bhalla. "Anisotropic in-plane strains and dielectric properties in $(\text{Pb,Sr})\text{TiO}_3$ thin films on NdGaO_3 substrates." *Applied Physics Letters* **84**, 577–579 (2004)

